Directional Analysis of Cardiac Motion Field based on the Discrete Helmholtz Hodge Decomposition

John A Sims[1,2], Maysa M G Macedo[2], Marco A Gutierrez[1,2]

[1] Laboratory of Biomedical Engineering, University of Sao Paulo, Sao Paulo, Brazil
[2] Division of Informatics, Heart Institute, University of Sao Paulo Medical School, Brazil

Abstract

The analysis of LV rotational motion could provide insights into myocardial dysfunction and predict the outcome of interventions, and this analysis could be performed more simply in separate rotational and radial components. In this study we present an automatic method for decomposing the cardiac motion field into radial and rotational components using the Discrete Helmholtz Hodge Decomposition (DHHD). The DHHD was applied to the following 3D motion fields (i) Synthetic complex motion fields, created by applying curl and gradient operators to Gaussian potentials, to determine numerical accuracy; (ii) Synthetic motion field from the 4D Extended Cardiac-Torso (XCAT) phantom (v2.0), to validate the use of the DHHD in decomposing cardiac motion fields. Decomposition error was found to decrease with increasing smoothness of the fields, while keeping motion field components small at the boundary of the motion field domain. The DHHD was seen to separate radial and rotational cardiac motion, allowing possible simplification of motion analysis.

1. Introduction

The cardiac left ventricular (LV) motion field can be quantified from image sequences showing LV motion through the cardiac cycle. Since disease can alter LV motion, the analysis of the cardiac motion field can assist in diagnosis.

Various methods can be used for cardiac motion field quantification, depending on the imaging modality. In previous work we showed how the 4D (3D + time) cardiac motion field can be estimated from gated single photon emisission computed tomography (SPECT) and positron emission tomography (PET) images using optical flow techniques [1] [2]. However, the analysis of cardiac motion fields, as a whole or in LV regions, can be a difficult and time-consuming task for the physician without assistance from specific software. One approach for motion field analysis produces indicators of cardiac health based on the magnitude of the motion field, such Kinetic Energy Index [1]. Although this information can be useful to medical teams, there is valuable information contained in the direction of the motion field which is not taken into account. Burns et al. [3] investigate the twisting motion present in normal LV function, concluding that an investigation of torsion may provide insights into myocardial dysfunction and help predict response to treatment. In this context, the separation of motion field components into radial and rotational motion could be used to present information in a manner which is simpler and easier to understand for medical teams. The separation of the cardiac motion field into these simpler components, which can be interpreted independently, facilitates an analysis of the motion field.

Directional LV motion analysis has been performed by transformation to cylindrical coordinates [4] or to spherical polar coordinates [5], both of which allow radial and rotational motion to be studied independently. However, the shape of the LV is neither spherical nor cylindrical, and the need for manual placement of the origin and alignment of the coordinate axes leads to operator-induced error.

The objective of this work is to demonstrate and validate a method for automated extraction of directional information relating to contraction, expansion and rotation of the LV.

2. Methodology

Polthier and Preuss [6] provide a tool for characterisation of flow topology called the Discrete Helmholtz Hodge Decomposition (DHHD), which uses a finite element approach to 2D vector field analysis. The DHHD was extended to 3D motion fields by Tong et al. [7], where the vector analysis is performed on a tetrahedralisation of the motion-field domain. In the decomposition, a smooth 3D vector field, $\vec{\xi}$, is written in terms of the sum of the gradient of a curl-free (CF) scalar potential, $[D]$, the curl of a divergence-free (DF) vector potential, $[\vec{R}]$, and a harmonic remainder, F_H, which is both CF and DF, as shown

in Equation 1.

$$\vec{\xi} = \nabla[D] + \nabla \times [\vec{R}] + F_H \quad (1)$$

2.1. Materials

The DHHD was applied to two types of 3D motion fields: (i) complex fields formed from the superposition of pure rotational and radial fields, created by applying differential operators to Gaussian potentials; (ii) a realistic cardiac motion field, generated from position vectors, which were output from the 4D Extended Cardiac-Torso (XCAT) phantom[8].

Field (i) allowed the variation of method error with input field smoothness to be studied. First Gaussian potentials, ϕ, were created on a $55 \times 55 \times 55$ voxel grid according to Equation 2 for eight values of standard deviation, σ, as shown in Table 1. A radial motion field was created by applying the gradient operator to the scalar potential, ϕ, and a rotational field in the xy plane by applying the curl operator to a vector potential with a non-zero z component, $(0, 0, \phi)$. The centre of the radial motion was set as the centre of the cubic grid and the central axis of the rotational motion passed through the centre of each xy slice The input vector field to the DHHD, $\vec{\xi}$, was created by summing a single counter-clockwise rotation and a single sink with no harmonic component. A slice through $z = 28$ of the motion field is shown in Figure 1, with the directional sense seen as looking along the z axis from positive z towards zero. In this figure, the central section has been amplified to show the summation of sink and rotation, and a region away from the centre, which shows a diminishing motion field away from the centre. The original radial and rotational components were saved as ground truth (GT) fields, $F_{CF\,GT}$ and $F_{DF\,GT}$, for performance assessment of the DHHD. Figure 2 shows the formation of $\vec{\xi}$ and GT fields.

$$ln(\phi) = -(1/2\sigma^2)[(x-x_c)^2+(y-y_c)^2+(z-z_c)^2] \quad (2)$$

Field (ii) allowed the use of the DHHD with cardiac motion fields to be validated. The parameter file for the XCAT phantom was set to generate 4D distribution emission radionuclide activity of the heart, simulating a 16 frame SPECT image with photon energy 140KeV, pixel size and slice depth of 0.3125cm. The volumes were of size $128 \times 128 \times 100$. The XCAT phantom offers the option to generate position vectors, allowing a motion field to be computed directly, as described below, rather than using techniques such as optical flow applied to the image sequence.

Generation of position vectors by XCAT provides voxel dislocation relative to frame one position. Only voxels which move from frame one position are present in the list of position vectors. So position vectors in frames 2 to 16 were converted to displacements from the previous frame to the current frame and position vectors were generated for each voxel of each frame, including null values. Next the velocity field was estimated in frames 2 to 15 using finite difference techniques as shown in Equation 3, where F is the motion field component calculated at position l, m, n in the grid for time frame t. P is the position vector in mm and δt is the time interval between frames, which was taken to have a value of one, providing units of $mm/frame$.

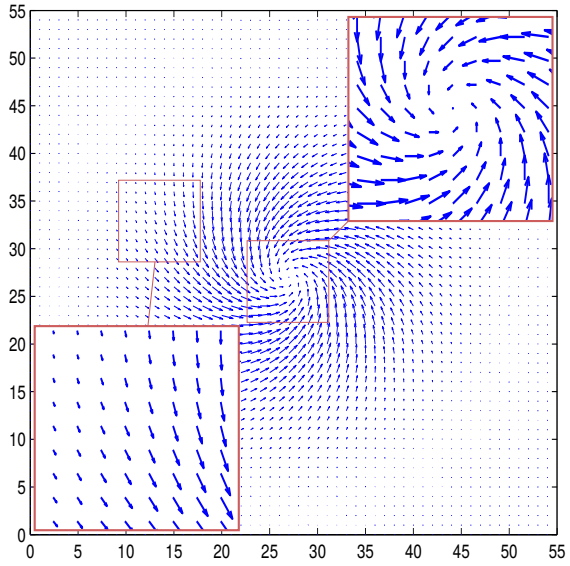

Figure 1. Slice through input field in xy plane with z=28, formed from a single sink and counter-clockwise rotation, with $\sigma = 7.071$, with two zoomed regions.

$$F^t_{l,m,n} = \frac{(P^{t+1}_{l,m,n} - P^{t-1}_{l,m,n})}{2\delta t} \quad (3)$$

2.2. Experiments

First the variation of method error with input field smoothness was studied using field (i). Motion fields, $\vec{\xi}$ were decomposed by the DHHD to form the CF and DF

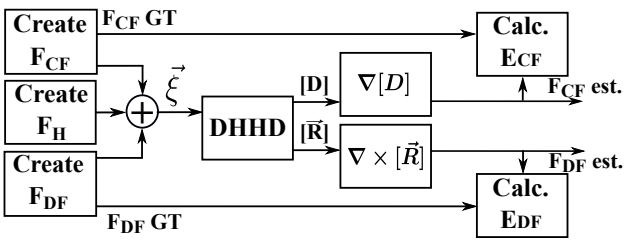

Figure 2. Performance evaluation of the DHHD

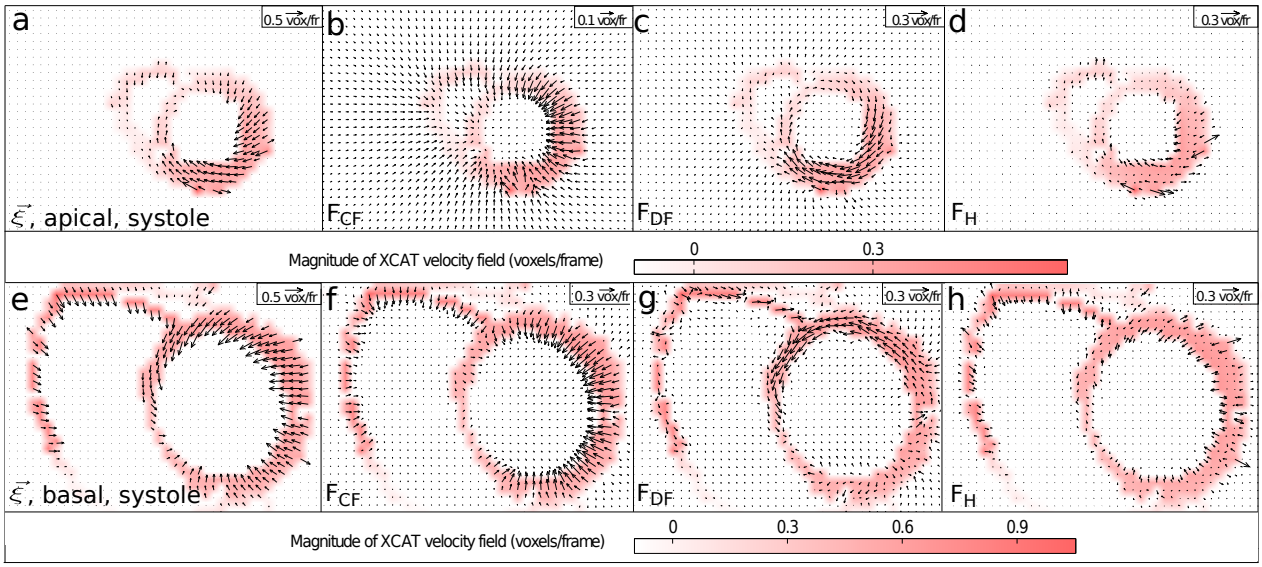

Figure 3. Decomposition of the XCAT motion field using the DHHD. The rows of the figure show motion fields for apical and basal systole. The first column shows the XCAT motion field obtained from XCAT position vectors, $\vec{\xi}$, and columns 2 to 4 show curl-free, divergence-free fields and the harmonic remainder, resulting from decomposition. The position of the myocardium, seen as the red-scale image in the figure, was estimated by taking the magnitude of the 3D Cartesian vector components composing the XCAT motion field. A slice in the short axis plane is shown in each figure.

potentials, $[D]$ and $[\vec{R}]$, from which estimated CF and DF fields, $F_{CF}\,est.$ and $F_{DF}\,est.$ were obtained. The GT and estimated fields for each of the CF and DF components were compared using the Normalised Root Mean Square Error (NRMSE) [9] to create error measures E_{CF} and E_{DF}, as shown in Figure 2.

Next the XCAT motion field, was decomposed into CF and DF components and the resulting fields visualised in systole and diastole, in both apical and basal short axis (SAX) slices. As shown in Equation 1, the harmonic field was calculated by subtracting the calculated CF and DF free fields from the input.

3. Results

Measured error in the DHHD was found to decrease with increasing standard deviation of Gaussian potential, reaching a minimum normalised RMSE of 0.87% and 1.01% for CF and DF components respectively with $\sigma = 7.071$. For larger values of σ, larger errors were found in the decomposition, as shown in Table 1.

Figure 3 shows the results of applying the decomposition to the XCAT motion field. The vector motion in the SAX plane has been overlaid on an approximate location of the myocardium, formed from the magnitude of the three components of the velocity field. The image slice and velocity field are shown according to an observer looking from the base towards the apex.

Frame 4 of the sequence was chosen to be representa-

Table 1. Variation of NRMSE with standard deviation of Gaussian potential for CF and DF motion fields created from the sum of a sink and counter-clockwise rotation.

Test	σ	NRMSE(%)	
		E_{CF}	E_{DF}
1	1.250	22.23	18.37
2	1.768	12.41	10.10
3	2.500	6.56	5.28
4	3.536	3.37	2.72
5	5.000	1.71	1.44
6	7.071	0.87	1.01
7	9.129	1.75	1.66
8	12.910	12.29	8.94

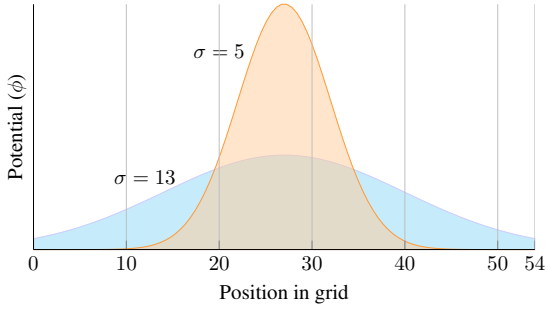

Figure 4. Smoothness of Gaussian potential on the grid and its value at the border for $\sigma = 5, 13$.

tive of systole, and slices were chosen near to the apex and base. The input motion field, ξ is shown in the first column, with the curl-free, divergence-free and harmonic remainder fields in the remaining columns.

4. Discussion

Figure 4 shows a one-dimensional representation of the Gaussian potential placed on the tetrahedralized grid for $\sigma = 5$ and 13. It is clear that increasing the standard deviation of the Gaussian potential results in a smoother motion field, but also in larger potential values at the border. The initial decrease of error in the decomposition shown in Table 1 correlates with increasing σ since the finite element approximations used in the DHHD become more valid [7]. However, the error increases greatly for larger values of σ since the motion field components at the domain boundary increase, causing artefacts in this region. If similar experiments were performed with different sized grids, an optimal value of $\frac{\sigma}{L}$ could be found, where L is the grid length, so that an appropriate value of σ could be chosen. Using the optimal value of σ from our experiments here, and the grid length 55, we estimate the value of $\frac{\sigma}{L}$ to be 0.129.

Decomposition of the XCAT field, as seen in Figure 3, produces CF and DF motion field components which clearly separate the radial and rotational motion. Our results are seen to be in line with Burns et al. [3], who predict anti-clockwise basal rotation and clockwise apical rotation in systole, seen from base looking towards the apex. Although figures showing diastole are not shown, the apex and base rotate in opposite directions to those in systole with similar radial motion, away from the centre of the LV. The XCAT field has sharp borders, which cause larger errors in the DHHD at the edges of the myocardium, reflected in the harmonic remainder fields (Figure 3 (d) and (h)) with large vectors at motion discontinuities of $\vec{\xi}$. The harmonic field, in the present case where there is an absence of large constant components, constitutes the method error.

The decomposition was performed on a motion field simulating nuclear medicine, but the motion field could, in principle, be obtained from any modality.

The DHHD provides an approach for performing an automated decomposition of directional components, producing radial and rotational motion as separate components. This could simplify medical analysis of the cardiac motion field. In future work, this directional analysis could be performed on quantified LV motion fields.

Acknowledgements

Thanks to University of Sao Paulo Support Foundation (FUSP) for their financial support, Professor Segars for his kind advice regarding the XCAT phantom and Dr A. Santiago for his advice regarding the implementation of the DHHD.

References

[1] Gutierrez MA, Rebelo MS, Furuie SS, Meneghetti JC. Automatic quantification of three-dimensional kinetic energy in gated myocardial perfusion single-photon-emission computerized tomography improved by a multiresolution technique. Journal of Electronic Imaging 2003;12(1):118–124.

[2] Sims J, Oliveira MA, Meneghetti JC, Gutierrez MA. Calculation of cardiac kinetic energy index from PET images. In MEDINFO 2015: eHealth-enabled Health - Proceedings of the 15th World Congress on Health and Biomedical Informatics, São Paulo, Brazil, 19-23 August 2015. 2015; 653–657.

[3] Burns AT, McDonald IG, Thomas JD, Macisaac A, Prior D. Doin' the twist: new tools for an old concept of myocardial function. Heart British Cardiac Society aug 2008;94(8):978–83.

[4] Rougon N, Petitjean C, Preteux F, Cluzel P, P. G. A non-rigid registration approach for quantifying myocardial contraction in tagged MRI using generalized information measures. Medical Image Analysis 2005;9(4):353 – 375.

[5] Rebelo M, Aarre A, Clemmesen K, Brando S, Giorgi M, Meneghetti J, Gutierrez M. Determination of three-dimensional left ventricle motion to analyze ventricular dyssyncrony in SPECT images. EURASIP J Adv Sig Proc 2010;.

[6] Polthier K, Preuss E. Variational approach to vector field decomposition. In de Leeuw W, van Liere R (eds.), Data Visualization 2000, Eurographics. Springer Vienna. ISBN 978-3-211-83515-9, 2000; 147–155.

[7] Tong Y, Lombeyda S, Hirani A, Desbrun M. Discrete multiscale vector field decomposition. volume 22. 2003; 445–452.

[8] Segars W, Sturgeon G, Mendonca S, Grimes J, Tsui B. 4d XCAT phantom for multimodality imaging research. Medical Physics 2010;37(9):4902–4915.

[9] Sims J, Furuie S, Gutierrez M. Automatic quantification of three-dimensional velocity field improved by spatially varying averaging filters. In XXIV Congresso Brasileiro de Engenharia Biomedica. 2014; p. 1937–1940.

Address for correspondence:

John Sims, Laboratorio de Engenharia Biomedica, PTC,
Escola Politecnica, University of Sao Paulo, Sao Paulo, Brazil
john.sims.incor@gmail.com